Surface Science 606 (2012) 1760–1770

Contents lists available at SciVerse ScienceDirect

Surface Science

journal homepage: www.elsevier.com/locate/susc

Characterization of 1*T*-$TiSe_2$ surface by means of STM and XPD experiments and model calculations

M.V. Kuznetsov [a,b,*], I.I. Ogorodnikov [a,b], A.S. Vorokh [a,b], A.S. Rasinkin [a], A.N. Titov [b]

[a] Institute of Solid State Chemistry, Ural Branch of the Russian Academy of Sciences, 620990, ul.Pervomaiskaya 91, Ekaterinburg, Russia
[b] Ural Federal University, 620002, pr.Mira 9, Ekaterinburg, Russia

ARTICLE INFO

Article history:
Received 20 January 2012
Accepted 14 June 2012
Available online 21 June 2012

Keywords:
Surface structure
Titanium diselenide
Scanning tunneling microscopy
Photoelectron holography
X-ray photoelectron diffraction
Surface relaxation

ABSTRACT

Scanning tunneling microscopy (STM) and X-ray photoelectron diffraction (XPD) are applied to study the surface of layered dichalcogenide 1*T*-$TiSe_2$. XPD pattern simulation for the 1*T*-$TiSe_2$ surface is performed in the approach of electron multiple scattering within the EDAC code: considered are models of structural defects in the 1*T*-$TiSe_2$ lattice, relaxation contraction (expansion) of surface layers and van der Waals gap, and deviation of the 1*T*-$TiSe_2$ surface geometry from the basal plane (001). The atomic structure of 1*T*-$TiSe_2$ surface layers is reconstructed from the XPD pattern on Se(LMM) and Ti2*p* core level using the photoelectron holography scattering pattern extraction algorithm with maximum entropy method (SPEA-MEM). The results of the 3*D* reconstruction are in agreement with the XPD pattern simulation data. In both cases, the $TiSe_2$ surface corresponds to 1*T* polytype; an increase is observed in the parameter a_0 and in the van der Waals gap between two surface slabs. It is assumed that similar structural distortions of the 1*T*-$TiSe_2$ lattice lead to the formation of an energy gap between the valence band and the conduction band of titanium diselenide, which was observed earlier by photoemission spectroscopy and follows from the theoretical calculations.

1. Introduction

The transition metal dichalcogenides, particularly, 1*T*-$TiSe_2$, have an apparently layered structure, in which the adjacent three-layer slabs (sandwiches) of chalcogen and metal atoms are separated with the van der Waals gap and are weakly coupled one with another. Owing to such structure, these compounds demonstrate a variety of interesting physical properties because of quasi-two-dimensionality of their crystal lattices. The properties of dichalcogenides vary widely upon intercalation with various atoms, molecules and even entire structural fragments into the interstices of the van der Waals gap [1–3]. Intrinsic structural imperfections affect the characteristics of these compounds as well. Thus, even high-purity single crystals reveal an excess titanium (over 0.2 at.%) that appears because of the crystal growth peculiarities. As a consequence, the dichalcogenides reveal vacancies in the crystal lattice on the sites of both chalcogen and titanium, with the titanium atoms partially filling in the interstices of the van der Waals gap [4]. A number of other structural defects are observed [5–7].

Scanning tunneling microscopy (STM) is one of the common methods for studying the atomic structure and structural defects on the surfaces of dichalcogenides [4–6,8–12]. This method has proved to be quite efficient, because the layered structure MeX_2 (X: S,Se,Te) allows easy preparation of structurally perfect and chemically pure surfaces via simple cleavage of the crystal along the van der Waals gap in the vacuum chamber of a microscope. Of a great interest are the ARPES experiments investigating into the electronic structure of TiS_2 and $TiSe_2$ compounds [13–15]. The depth of the ARPES analysis penetrates to a few surface layers only and is extremely sensitive to the presence of chemical impurities and to the surface structure of the material under study. Samples for the ARPES are prepared by cleaving a single crystal in vacuum; and one can assume that the structural defects imaged by STM are also present on the surface and contribute into the ARPES results. Based on the calculation results [16] evidenced by the ARPES data, the TiS_2 and $TiSe_2$ dichalcogenides possess a narrow energy gap between the valence band, which is formed by the S3*p*(Se4*p*)-states of the chalcogen, and the conduction band, which is formed by the Ti3*d*-states of titanium [17,18]. Therefore, these dichalcogenides are semiconductors. At the same time, in terms of the bulk characteristics, the $TiSe_2$ compound should rather be regarded semimetal [19]. This contradiction was studied in [20]. It was demonstrated that the width of the energy gap between the valence band and the conduction band depends on the number of layers (slabs) in the simulated films of TiS_2 and $TiSe_2$: for a three-layer fragment (slab) X-Ti-X, the energy gap is 1.0 eV; when the number of slabs reaches 11, the energy gap narrows and the TiX_2 film becomes a semimetal. Such dependence of the electronic structure

* Corresponding author at: Institute of Solid State Chemistry, Ural Branch of the Russian Academy of Sciences, 620990, ul.Pervomaiskaya 91, Ekaterinburg, Russia. Tel.: +7 343 3623356; fax: +7 343 3744495.
E-mail address: kuznetsov@ihim.uran.ru (MV. Kuznetsov).

0039-6028/$ – see front matter © 2012 Elsevier B.V. All rights reserved.
doi:10.1016/j.susc.2012.06.008

on the TiX_2 film thickness emphasizes the importance of studying the surfaces of these layered compounds. In particular, it is crucial to know the scope of relaxation deformation of the surface layers of titanium dichalcogenides, for instance, at the expense of expansion (contraction) of the van der Waals gap between the top structural slabs of X-Ti-X or as a result of alteration in the lattice parameters inside the first slab.

One of the possible ways of surface deformation is a slight distortion of the topmost slab, which leads to the alteration in the local environment of the titanium atom with chalcogen atoms. As demonstrated in [21], the gap between the S(Se)*p*- and Ti3*d*-bands is controlled by the value of splitting of Ti3*d*-orbitals in the crystalline field. An increased splitting results in a decrease in the energy of the lowest Ti3d_{z^2}-orbital and in its overlapping with the top of the valence band. The amount of splitting is determined by the symmetry of the local environment of a titanium atom, which is numerically characterized as the ratio of lattice parameters c_0/a_0. The coordinate *z* of selenium atom along the normal to the basal plane is assumed to be 0.25, which means the equality between the width of the slab and the van der Waals gap. According to [22], for TiS_2 and $TiSe_2$ compounds such approximation is quite right. Increasing of the c_0/a_0 ratio provides lowering in the symmetry of the local environment and increasing of the splitting of Ti3*d*-orbitals. Therefore, deformation of the outer layer due to its expansion along the basal plane or due to its contraction along the normal to that plane can lead to the reduction in the c_0/a_0 ratio thus providing the S(Se)*p*/Ti3*d* gap observed.

The present study investigates into the cleaved surface of 1*T*-$TiSe_2$ single crystal using the STM, X-ray photoelectron diffraction (XPD) and photoelectron holography [23–26], in order to reveal whether the surface layers of this dichalcogenide can really be deformed and what are the scopes of the structural distortions to be. The depth of XPD analysis amounts to several nanometers and in this regard the method is adding the STM data with information about the layers lying immediately below the surface of solids. The physical nature of X-ray photoelectron diffraction allows the XPD patterns of photoelectron or Auger emission from atoms of this or that sort located in the surface layers to be viewed as holograms, similarly to holographic images in optics. As a reference wave acts the electron wave that has achieved from the emitter atom to the electronic analyzer without scattering on the emitter's nearest neighbor atoms. Accordingly, an object wave is formed at the expense of the scattering of electrons on the surrounding atoms. In this paper we made an effort to use the SPEA-MEM [27] formalism for reconstruction of the structure of 1*T*-$TiSe_2$ surface layers from the XPD pattern on Se(*LMM*) and Ti2*p* core level.

2. Experimental part and calculation models

Single crystals of 1*T*-$TiSe_2$ were grown by gas-transport reactions via the method of direct sublimation of previously synthesized polycrystalline materials in a vacuumed quartz ampoule. The crystals were shaped as plates (5×5 mm) of up to 0.3 mm in thickness. The STM measurements were carried out using a VT-STM Omicron scanning tunneling microscope with a tungsten tip at room temperature; when recording the images, the bias voltage applied to the tip was $U=-0.1$ V, the tunneling current $I=1$ nA. Before the experiment, the crystals with metal columns attached to the surface were placed in a vacuum chamber of the scanning tunneling microscope (at a vacuum of 10^{-8} Pa). Using a mechanical manipulator, the columns were torn off the crystal surface thus a dichalcogenide's surface layer was peeled off and a clean surface of the crystal was revealed. Since the cleavage occurred exclusively along the van der Waals gap, the resulted surface corresponded to the plane (001) 1*T*-$TiSe_2$.

The experiments on X-ray photoelectron diffraction on the 1*T*-$TiSe_2$ surface were carried out using an ESCALAB MK II spectrometer with the use of nonmonochromatic radiation Al *K*α ($E_{h\nu}=1486.6$ eV). The electron spectrometer was combined with a scanning tunneling microscope, so the same samples of 1*T*-$TiSe_2$ were used for XPD, XPS and STM experiments. Composition of the surface was controlled by means of the X-ray photoelectron spectroscopy (XPS). It is established that along with the lines corresponding to the basic elements (Ti, Se), the XPS spectra reveal low intensity maxima attributed to O1*s*-oxygen and C1*s*-carbon.

The XPD experiment was performed on a fresh cleaved surface of 1*T*-$TiSe_2$ crystal. In the photoelectron spectrum of this dichalcogenide, the lines of greatest intensity are attributed to Ti2*p*-electronic states of titanium, with the kinetic energy of ~1030 eV, and the band of Auger transition on the selenium atoms Se($L_3M_{45}M_{45}$), for which E_{kin} ~1310 eV. These lines were selected for recording the XPD patterns of titanium and selenium. In our XPD theoretical calculations for titanium, we considered photoelectrons emitted from the Ti2*p* levels, and in the calculations of Auger electron diffraction of Se($L_3M_{45}M_{45}$) we used emitted waves with *f* angular momentum [28]. To be exact, the XPD stands for X-ray photoelectron diffraction; in our report, however, we use this abbreviation to also mean diffraction of Auger electrons of Se(*LMM*) emission excited by X-ray radiation.

The XPD patterns for Ti2*p* and Se($L_3M_{45}M_{45}$) were constructed as follows. A 1*T*-$TiSe_2$ single crystal was mounted on a sample holder in the chamber of the spectrometer analyzer. The sample was oriented in the chamber relative to the axis of electronic analyzer. The solid angle of the electron collection was ~0.3°. In the course of the XPD experiment, the 1*T*-$TiSe_2$ crystal was rotated step-by-step over polar and azimuthal angles, with a scanning step of 2.5° and 5° for Se(*LMM*) and Ti2*p*, respectively. The spectra of the selected lines were recorded upon each scanning step.

For calculations of photoelectron diffraction, we utilized the EDAC (Electron Diffraction in Atomic Clusters) cluster-model approach developed by F. Javier Garcia de Abajo, Michel A. Van Hove and Chuck Fadley in the Lawrence Berkley National Laboratory (California, USA) on the basis of the spherical wave multiple scattering (MSC-SW) approximation for a selected cluster [26]. This approach allows computation to be performed on large clusters of a size up to several thousand atoms using iterative procedures ensuring rapid convergence of results. Simulation of photoelectron diffraction is carried out with due account for the *muffin-tin* potential and calculated phase shifts.

In the work presented, in order to simulate XPD on the $TiSe_2$ surface, clusters of parabolic shape were used (Fig. 1) [26]. The size and shape of a cluster were determined by the value $R_{max}\geq|r_i-r_0|+(z_{surf}-z_i)$, which was chosen to be approximately 1.5 times as great as the mean free path of an electron with an energy of ~1300 eV in $TiSe_2$. Here, r_i and r_0 are radius vectors of the *i*-scatterer atom and emitter atom, respectively; z_{surf} and z_i are the coordinates in the direction of the normal to the surface and of the *i*-scatterer, respectively. The number of atoms in the cluster was varied from ~300 to

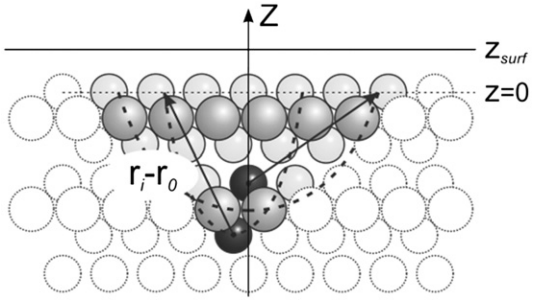

Fig. 1. Schematic representation of a cluster of $TiSe_2$ structure used for computing XPD by EDAC approach.

~1000 depending on the depth at which the emitter atom lies relative to the crystal surface.

For reconstruction of the atomic structure of the 1*T*-$TiSe_2$ surface from the XPD pattern in Se(*LMM*) and Ti2*p* emission, an approach recently suggested by T. Matsushita et al. [27] was used, which is not based upon Fourier transform from the reciprocal space to the real space but rather utilizes the scattering pattern extraction algorithm and maximum entropy method (SPEA-MEM). This approach takes into consideration the phase shifts and allows images of atoms to be extracted from a single diffraction pattern. To save time needed for computations and to acquire clear images of atoms, we excluded the reciprocal scattering region and took into account the sixth-order symmetry of the 1*T*-$TiSe_2$ layers. Because two inequivalent positions of Se atoms can be distinguished on the 1*T*-$TiSe_2$ diselenide surface (in a three-layer slab Se–Ti–Se, there are different positions of Se atom in the upper and lower layers), the resulted pattern was built as a superposition of two reconstructed images of each of the inequivalent Se atoms.

3. Results and discussion

3.1. Scanning tunneling microscopy of the cleaved surfaces of 1T-TiX_2 (X: S,Se) single crystals

Currently available STM experiments performed on the surfaces of freshly cleaved 1*T*-TiX_2 (X:S,Se) crystals [4,5,9,12] demonstrate that, along with the point defects, e.g., vacancies on the chalcogen sites, there are other, more intricate arrangements of sulfur or selenium atoms in the form of triangles rising from the surface. Fig. 2 displays examples of the STM images with such defects, which we acquired on the cleaved surfaces of 1*T*-$TiSe_2$ and 1*T*-TiS_2. It is seen that on the (001) surface of 1*T*-TiS_2 disulfide, there are point defects, i.e., vacancies

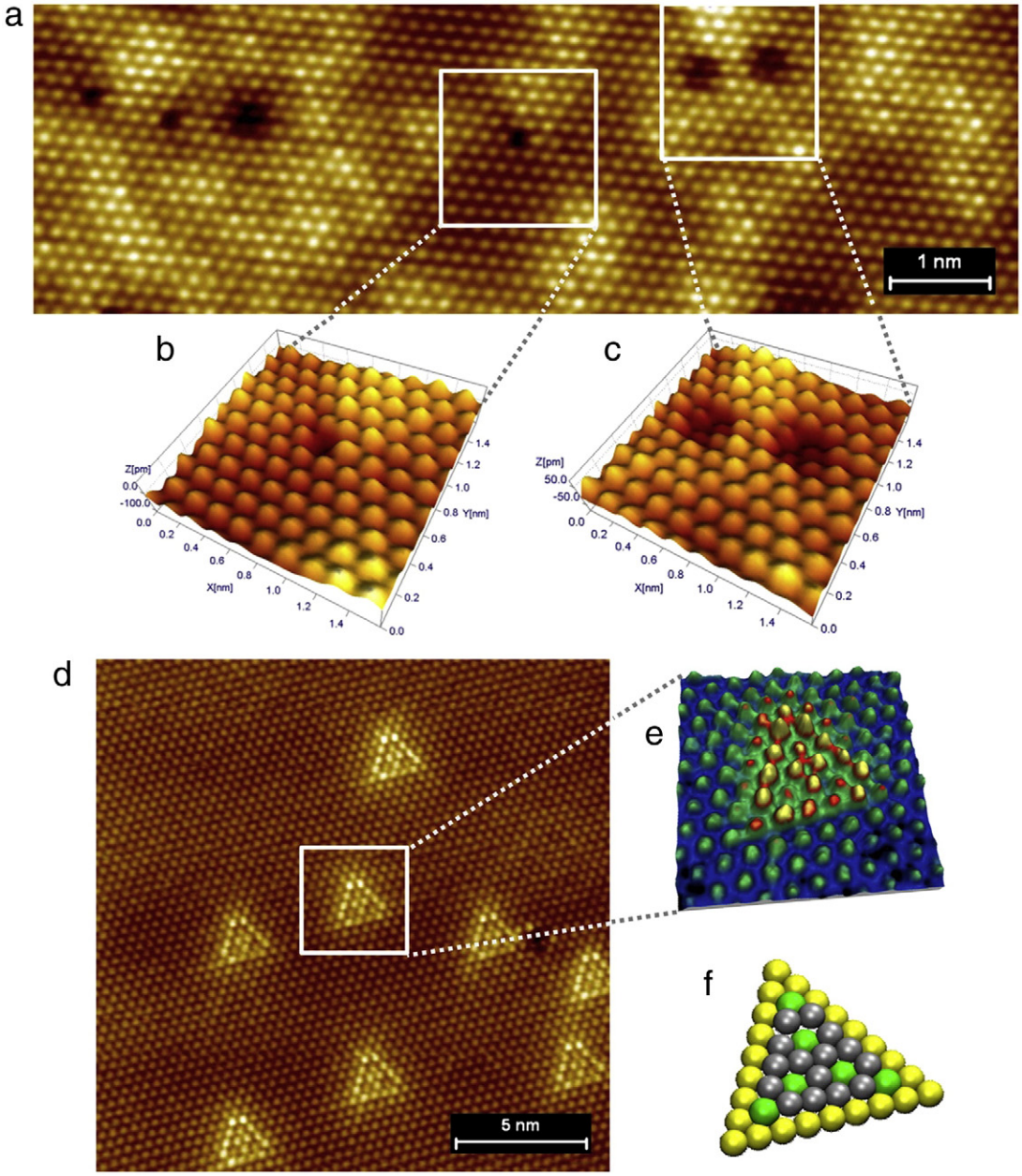

Fig. 2. STM images: 1*T*-TiS_2 surface 3×10 nm^2 (a), marked areas with atomic defects are shown in 3*D*-images (b) and (c); 1*T*-$TiSe_2$ surface 20×20 nm^2 (d), marked area with triangular defect (e) and 3*D*-modeling cluster (f).

on the lattice sites of sulfur atoms on the background of large triangular formations (Fig. 2b). Additionally, there are also defects comprising three sulfur atoms, which are imaged by STM as lying beneath the plane of the top layer of the crystal. The nature of this type of defects is not obvious and calls for model calculations (Fig. 2c). On the 1*T*-$TiSe_2$ surface, the concentration of point defects (vacancies on Se sites) is considerably lower (see Fig. 2d). With this observed, equivalently oriented triangular structures are clearly seen in the (1×1)-lattice of the outer Se-layer containing clusters of selenium atoms (the atomic clusters $6\times6\times6$). Selenium atoms forming the structures belong to the first layer of diselenide, however, they are rising from the surface by tenths of an angstrom. In this case, by saying "rising" from the surface we assume in favor of the geometrical factor of the STM imaging, however, it should be understood as not quite correct. The triangular Se-clusters have their own substructure, wherein selenium atoms are located at various heights relative to the crystal surface. We determined the average positions of each of the Se atoms in the eight triangles observed relative to the selenium positions on the surface and built a three-dimensional model of such cluster on the surface (Fig. 2f). It is seen that the structures visualized as triangles in reality consist of three conjugate hexagons, with selenium atoms located in their vertices. At an average, such a cluster is rising from the surface by ~0.3 Å, with the height of two Se-atoms over the surface being 0.5 Å.

There are several explanations for the nature of such superstructures observed by STM. For example, the authors of [4,5], relate such superstructures to vacancies or Frenkel defects on titanium sites below the first top layer of selenium atoms and to part of the titanium atoms migrating in the van der Waals gap. In our study [29] we made an effort to explain such superstructures by the structural defects of the type 2*H*-TiX_2, in which the octahedral coordination of titanium atoms changes into the prismatic orientation. When comparing the STM images with the calculations, only the geometry factor was taken into consideration, i.e., the relaxation displacements of atoms in the vicinity of the defect relative to their sites in the 1*T*-TiX_2 lattice. As of today, however, it is not fully understood whether the triangular structures observed on the STM images of dichalcogenides are attributed to intrinsic defects, for instance, to growth defects, or they are formed during the mechanical cleavage of the crystal along the basal plane.

To sum up the resulted STM data for the cleaved surface of 1*T*-$TiSe_2$ crystal, the following conclusions can be made: *i*) the crystal is cleaved along the van der Waals gap to form the (001) surface consisting of selenium atoms; *ii*) the surface is 1*T*-type $TiSe_2$; *iii*) the amount of point defects in the form of vacancies on the selenium sites is extremely small; and *iv*) there are superstructures present on the surface in the form of three conjugate hexagons of Se atoms rising above the surface by $0.3\div0.5$ Å. Again, the nature of these superstructures is not clearly defined: it can be associated with part of Ti atoms migrating from their sites in the Se–Ti–Se slab into the interstices of the van der Waals gap or it can be explained by the local transformation of the structural arrangement inside the Se–Ti–Se slab from 1*T*-$TiSe_2$ to 2*H*-$TiSe_2$. In any case, these defects are of great interest so far as they alter the local electronic density of the surface and, consequently, affect its local chemical behavior [4].

However, the STM is known to have its limitations. It allows only the atoms of the topmost surface layer to be imaged; in our case, they are the chalcogen atoms. In principle, the STM is capable of providing information about the structural defects located under the surface. In this case, the use is made of the relaxation effect of displacement of the surface atoms near the defect, and of the variation in their charge state. The problem is that both these factors (the relaxation displacement of atoms and the local electron density variation) determine the tunneling current between the surface and tip, and together form an STM image. Therefore, the reason for higher or lower brightness of this or that region or atom on the STM pattern is not always clear: this can happen due to the change in both the geometrical positions of atoms and the electron density on the atoms.

3.2. X-ray photoelectron and Auger electron diffraction of the 1*T*-$TiSe_2$ surface

To analyze the atomic structure of layers located immediately under the (001) surface of 1*T*-$TiSe_2$, we used the photoelectron and Auger-electron diffraction holography methods. Fig. 3 displays experimental XPD patterns of emission on Se($L_3M_{45}M_{45}$) and Ti2*p* core level from the cleaved surface layers of 1*T*-$TiSe_2$ crystal within the polar angle ranges of $0\div70°$ (for Se(*LMM*)) and $0\div65°$ (for Ti2*p*) relative to the surface. The diffraction patterns are built similarly to stereographic projections and are represented in the gradations of gray. The resulted XPD images have symmetry characteristic of the trigonal lattice (space group $P\bar{3}m1\left(D_{3d}^3\right)$; clearly seen is a "triangle", the sides of which lie on the Kikuchi lines formed at the expense of atoms located in the close packed planes of the titanium diselenide lattice.

Similar patterns for XPD Se3*d* and Ti2*p* of the $TiSe_2$ surface were obtained and discussed in [30]. To interpret the experimental XPD patterns, the authors of [30], based on the model calculations in the single scattering approximation (*SSC-SW*), made a conclusion about a good agreement between theory and experiment and confirmed the fact that the $TiSe_2$ crystal is cleaved along the van der Waals gap

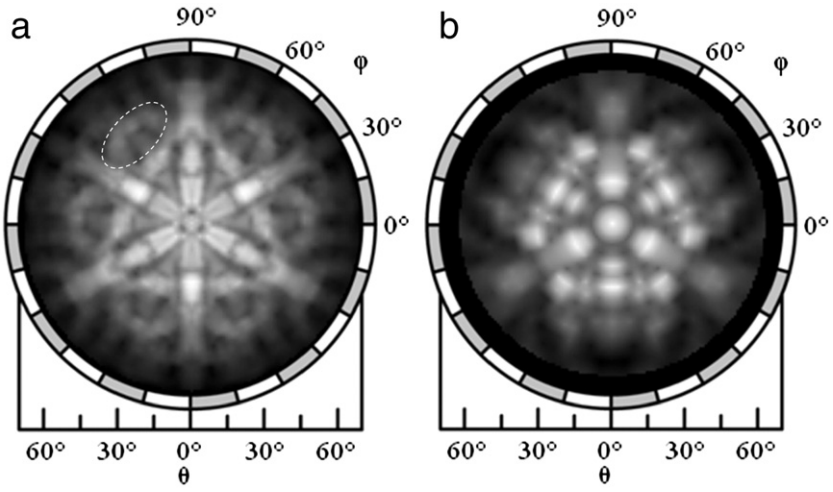

Fig. 3. Stereographic XPD projections: a — Se(*LMM*) ($E_{kin}=1310$ eV); b — Ti2*p* ($E_{kin}=1030$ eV). Bright regions are of high intensity; dark regions are of low intensity.

with Se-terminated surface. The conclusion on the cleavage along the basal plane is obvious as it follows from the numerous STM experiments with these layered compounds. Theoretical analysis of the XPD patterns, in particular, fitting the model calculations with the experimental 2π-projections is more complicated. The matter is that the layered character of dichalcogenide structure enables the existence of such structures in a variety of polytypes. Known are the 1*T*, 2*H*, 3*R*, 4*H* polytypes, etc., where digits denote the number of $TiSe_2$ layers in the unit cell and the letters denote the lattice type: *T* for tetragonal, *H* for hexagonal and *R* for rhombohedral. The polytypes may have modifications, such as 2*Ha*, 2*Hb*, and 2*Hc*, which differ in the sequence of $TiSe_2$ layers. The 2*H* polytype is of interest because of the possible involvement (judging from the STM data) of the structural fragments of this type on the surface of 1*T*-$TiSe_2$ crystal [29]. In the present work, when simulating the photoelectron diffraction of Se($L_3M_{45}M_{45}$) electrons, we confined ourselves with consideration of the basic polytype 1*T*-$TiSe_2$, the hexagonal polytype 2*H* and a number of its modifications such as 2*Ha*, 2*Hb* and 2*Hc*.

Fig. 4 displays the 1*T*-$TiSe_2$ crystal structure, a stereographic projection of the principal crystallographic directions for the basal plane (001) of the crystal, and an EDAC approach-computed pattern of diffraction of Se(*LMM*) electrons in the lattice of the 1*T*-$TiSe_2$ surface layers. Superposition of the stereographic projection on the XPD pattern demonstrates their good correlation. A conclusion can be made that, firstly, the calculations based on the EDAC approach in the multiple scattering approximation describe diffraction of Se(*LMM*) electrons on the $TiSe_2$ surface, and, secondly, the *in forward direction* approximation works well for the kinetic energy of electrons E_{kin} ~ 1310 eV.

On the stereographic projection (Fig. 4b), shown with triangles and circles are the scattering reflections of Se(*LMM*) electrons on titanium and selenium atoms of the first and second coordination spheres. The size of a reflection is determined by the distance between the planes of emitter atom and scatterer atom. Therefore, when analyzing a diffraction pattern, one can identify the structural positions of emitter and scatterer atoms, which define this or that reflection on the 2π-projection of XPD.

Comparison of the experimental XPD pattern of scattering Se(*LMM*)-electrons on the $TiSe_2$ surface (Fig. 3a) with the theoretically calculated XPD pattern (Fig. 4c) was performed based on computing of their reliability *R*-factor:

$$R = \frac{1}{n}\sum_n \sum_m \left| I^{\exp}_{n,m} - I^{th}_{n,m} \right| \Big/ \sum_m \left| I^{\exp}_{n,m} \right|, \quad (1)$$

where *n* is the number of azimuthal angular dependence (i.e. the number of scanning steps over the azimuthal angle) and *m* is the number of polar angular dependence (i.e. the number of scanning steps over the polar angle). The lower the *R*-factor, the better is the agreement between experiment and theory. In our case, the *R*-factor amounted to 0.0567, which is evidence of a good agreement between the model calculations and experiment. However, one can see that the experimental XPD pattern of Se(*LMM*) is somewhat different from the theoretically calculated XPD pattern in the polar angle region 45 ÷ 55°. In this region, the experiment reveals the characteristic features in the form of "petals" (marked in Fig. 3a), which are not seen so clearly in the simulated XPD patterns.

To reduce the effect of noise at large polar angles, the authors of [31,32] suggested that the *R*′-factor be calculated by the following equation:

$$R' = \sum_n \left| \chi^{\exp}_n - \chi^{th}_n \right| \Big/ \sum_n \left| \chi^{\exp}_n \right|, \quad (2)$$

where the normalized angular anisotropy $\chi_n = |I^{\max}_n - I^{\min}_n| / I^{\max}_n$, and *n* is the number of azimuthal angular dependence (i.e. the number of scanning steps over the polar angle). The *R*′-factor calculated by Eq. (2) equals to 0.157. Both the approaches to *R*-factor calculation were used in order to find optimal parameters of the $TiSe_2$ surface structure.

In general, to agree theory with experiment, one should carry out a complicated many-parameter analysis with optimization of the model cluster geometry and searching for a global minimum of the *R*-factor. That is quite a laborious task. We confined ourselves with consideration of some examples that demonstrate the sensitivity of *R*-factor to variation of a number of geometry parameters of the crystal structure of dichalcogenide. In a simple case, a change in the surface structure can be caused by relaxation contraction (expansion) of the interatomic bonds. Simulation of relaxation of 1*T*-$TiSe_2$ surface structure was carried out by varying the lattice parameters a_0 and c_0. The parameter a_0 is the interatomic distance in the layer of Ti or Se inside the Se–Ti–Se topmost slab. A deviation of parameter c_0 from its bulk value is determined as by contraction (expansion) of the van der Waals gap (*D*) as by alteration of the Se–Ti interatomic distances (*d*) in the topmost slab. Fig. 5 displays the surfaces of *R*-factors calculated by Eqs. (1) and (2) and constructed for a massive of variables: $\Delta D/D = -20 \div +50\%$, $\Delta d/d = 0 \div -35\%$, $a_0 = 3.53 \div 4.13$ Å.

In this case, the parameter c_0 changes in the range of ±20% of its bulk value. In the figure, the percentage of contraction of Se–Ti interatomic distances (*d*) inside a slab and the van der Waals gap (*D*)

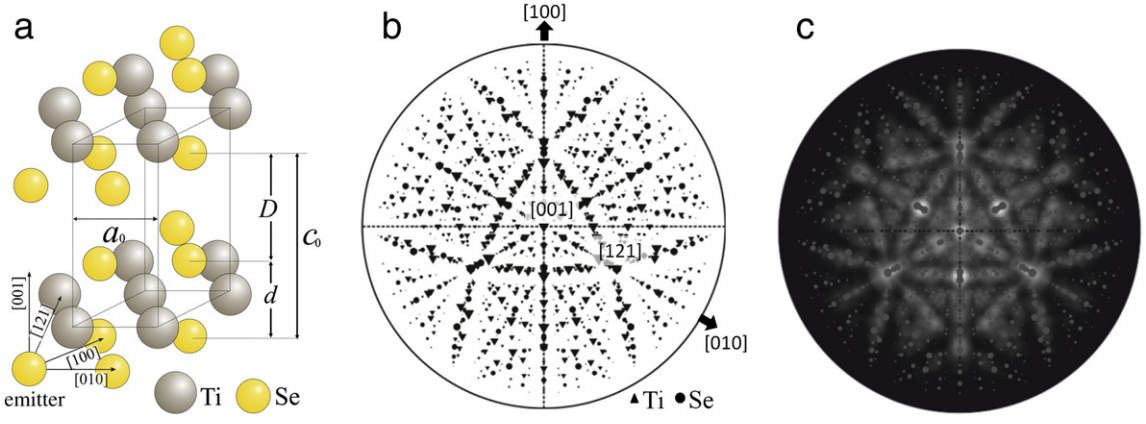

Fig. 4. (a) Structure of 1*T*-$TiSe_2$, space group $P\bar{3}m1$ ($a_0 = b_0 = 3.535$ Å, $c_0 = 6.004$ Å, $d = 3.450$ Å, $D = 2.554$ Å). (b) The stereographic projection of scattering *in forward direction*: triangles denote the scattering directions of Se(*LMM*) electrons on titanium atoms, and circles denote the scattering directions of Se(*LMM*) electrons on selenium atoms. (c) Calculated XPD pattern of the 1*T*-$TiSe_2$ surface in the polar angle range 0 ÷ 90° with superimposed reflections of the stereographic projection; the calculations were carried out using the EDAC approach in the multiple scattering approximation of Se(*LMM*)-electrons with $E_{kin} = 1310$ eV.

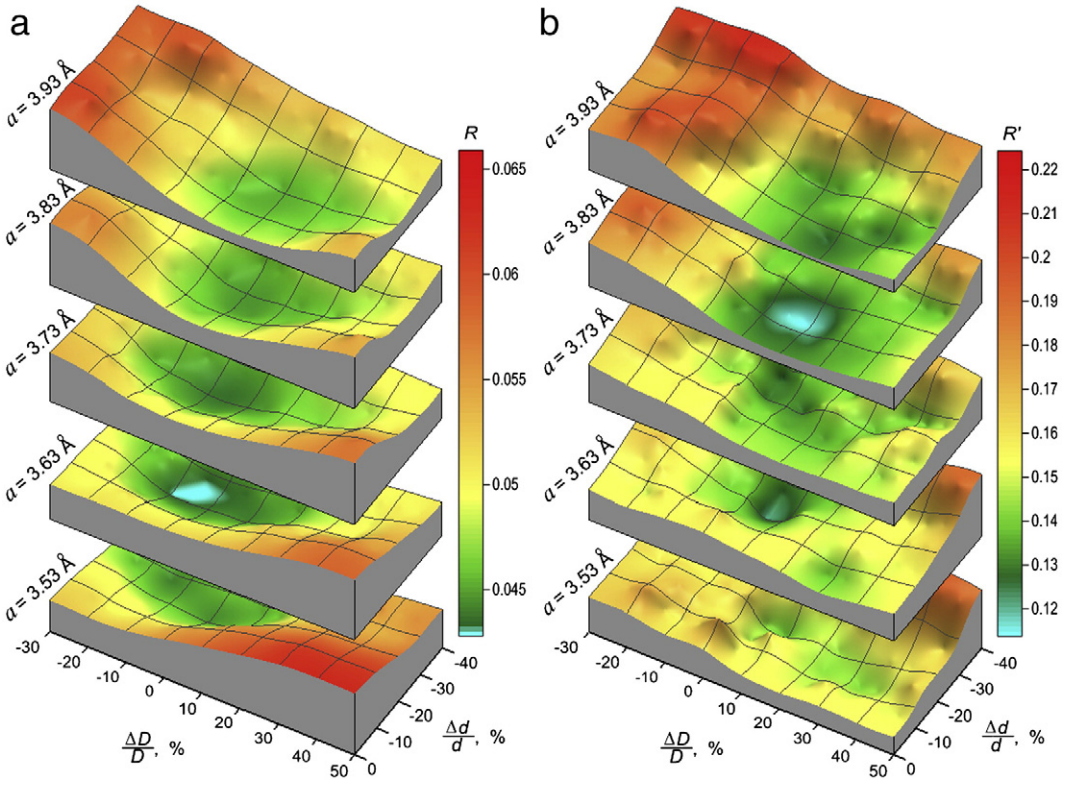

Fig. 5. Values of *R*-factor calculated by Eq. (1) (a) and of *R*′-factor calculated by Eq. (2) (b) showing the agreement between the experimental and simulated XPD Se(*LMM*) patterns for 1*T*-$TiSe_2$ surface. Plotted along the *y* and *x* axes are the values of contraction (%) of the Se–Ti distances inside a slab (*d*) and the van der Waals gap between slabs (*D*). Plotted along the *z* axis is the *R*-factor. The *R*-surfaces correspond to various lattice parameters *a*: there are five *R*-surfaces represented for $a = 3.53 \div 3.93$ Å.

between slabs are plotted along the *x* and *y* axes, with the *R*-surfaces corresponding to the various values of parameter a_0 of the diselenide lattice. One can see that the *R*-factor calculated by Eq. (1) reaches its minimum $R = 0.043$ at a contraction of the van der Waals gap by $\Delta D/D = -6 \pm 3\%$, at a decrease of the Se–Ti distance in the first slab by $\Delta d/d = -21 \pm 5\%$ and at a slight increase in the a_0 parameter up to 3.63 Å. In the case that the Eq. (2) is applied, the minimum $R' = 0.12$ is obtained at $\Delta D/D = 5 \pm 3\%$, $\Delta d/d = -21 \pm 4\%$, and $a_0 \sim 3.63$ Å. Evidently, the two approaches to *R*-factor calculation yield close results for *d* and a_0 and demonstrate an opposite effect of contraction (expansion) of the van der Waals gap. In addition to the minimum value observed approximately in the same region of *R*- and *R*′-surfaces, there is an additional global minimum observed at $R' = 0.11$ with $\Delta D/D = 19 \pm 3\%$, $\Delta d/d = -14 \pm 3\%$ and $a_0 \sim 3.83$ Å. When calculating the *R*-factor by Eq. (1), this minimum is not pronounced so clearly. In the case that the additional minimum is observed, considerable distortions of the $TiSe_2$ surface structure can be suggested: the van der Waals gap increases, the Se–Ti–Se slab contracts, and the lattice parameter a_0 grows. In general, it turns out that, in the attempt to determine the parameters of 1*T*-$TiSe_2$ surface structure from the minimum *R*-factor, we have encountered the uncertainty in making the correct final choice. In solving this issue, the photoelectron holography data are of great help, which will be discussed below. In anticipation it should be noted that these data provide evidence in favor of the additional global minimum, at which the lattice parameter a_0 in the Se–Ti–Se slab near the surface increases up to ~3.83 Å. Comparing the two approaches to the *R*-factor calculation by Eqs. (1) and (2), we have come to a conclusion that the algorithm (2) estimates the *R*-factor at a higher accuracy and generally yields more exact results. Hence, in our further considerations we shall use the *R*′ factor calculated by Eq. (2).

Therefore, the performed XPD calculations demonstrate that, if we acknowledge the relaxation contraction (expansion) of the 1*T*-$TiSe_2$ surface layers and the alterations in the interatomic distances inside the topmost slab, then the best agreement with experiment is attained at the van de Waals gap increased by ~19% relative to its bulk value, at the contraction of the topmost slab by ~14%, and at the increased lattice parameter a_0 of the topmost slab up to 3.83 Å, which is by 0.3 Å greater than the lattice parameter in the bulk of diselenide. It should also be considered that the lattice parameter c_0, which is equal to the sum of *D* and *d*, grows by ~1% in the surface layer. It should be noted that accuracy of the XPD analysis is not great during computing of the relaxation contraction (expansion) of the lattice in the surface layers, and in our case it is determined with a rather large scanning step by the angles in the XPD experiment ($\Delta\theta,\varphi = 2.5°$).

The result thus obtained agrees with a conclusion made in [33], where the XPD method was applied to explore a related system of 1*T*-TaS_2 compound. There, the authors came to the conclusion that in the surface layers the lattice parameter c_0 of 1*T*-TaS_2, which comprises the van der Waals gap and the thickness of the S–Ta–S slab, is 2% greater as compared to the lattice parameter of the bulk crystal. Additionally, our XPD experiments on the $TiSe_2$ indicate a possibility of rather considerable distortions in the upper layer (topmost slab) of the diselenide: the thickness of slab is reduced and the interatomic distances are extended in the basal plane of the crystal. Note that it is such distortions that can result in the formation of an energy gap between the valence gap and the conduction gap of titanium diselenide, which is evidenced by ARPES and follows from the theoretical calculations [13,15,22].

If, however, the assumption can still be made that the surface layers of 1*T*-$TiSe_2$ do not undergo considerable relaxation distortions, then reasons should be sought, why the distortions exist on the surface on the real crystal and are revealed by the XPD experiment. One of such reasons can be the defects, which are always present in the crystal's bulk and, surely, on the crystal's surface. Below we

consider how such defects – structural and topological – can hypothetically affect the photoelectron diffraction patterns of the 1*T*-$TiSe_2$ surface.

So far as we do not discount a possibility that one of the defects on the surface of dichalcogenide can be the structural fragment of 2*H*-polytype [29], we tried to simulate XPD patterns of the 1*T*-$TiSe_2$ crystal surface with similar macroscopic defects. Fig. 6 displays an XPD pattern of a $TiSe_2$ cluster with 1*T*-type of structure, in which the surface slab Se-Ti-Se has the 2*H*-arrangement. Ambiguity of the agreement between the surface 2*H*-layer and the substrate composed of 1*T*-$TiSe_2$ layers results in six alternative versions of the arrangement, when titanium and selenium atoms are located in the positions as AbA AbC, AcA AbC, BaB AbC, BcB AbC, CaC AbC, and CbC AbC (where a capital letter denotes the selenium atom, and a lower case letter denotes the titanium atom).

Fig. 6 displays the diffraction pattern of Se-electrons scattered on such hypothetical structures. One can see that none of the versions can adequately describe the experimental XPD pattern of Se(*LMM*)-emission (see Fig. 3a), possibly with the exception of a — AbA AbC, when the *R*′-factor decreases down to 0.130. It should not be surprising, because density of such structural defects on the 1*T*-$TiSe_2$ surface is small, and only motifs of the simulated patterns should be expected on the experimental XPD patterns of real crystals. If such motifs are revealed, then this fact will support the hypothesis of 2*H*-inclusions present in the structure of a cleaved surface of 1*T*-$TiSe_2$.

Indeed, if we introduce a structural defect in the form of 2*H* polytype into a model cluster of 1*T*-$TiSe_2$ (Fig. 7a,b) filling in approximately 13.4% of the cluster's surface area, then the theoretically calculated XPD pattern of Se(*LMM*) emission (Fig. 7d) shows the best agreement with experiment. With this observed, in the case that the *R*′-factor is calculated by Eq. (2), the minimum value $R' = 0.126$ is obtained when the defect is located in first slab at the surface 1*T*-$TiSe_2$. It will be recalled that without the defect and surface relaxation taken into consideration, the *R*′-factor amounted to $R' = 0.157$. Therefore, structural defects in the form of 2*H* polytype (if actually present on the 1*T*-$TiSe_2$ surface) can in principle be regarded as an alternative to the model of relaxation contraction (expansion) of surface layers of diselenide, and in both cases the reliability *R*′-factor can be reduced indicating the agreement between theoretical and experimental XPD patterns. The result can be improved if, along with the defect introduced into the model, the structural parameters (D, d, a_0) of the 1*T*-$TiSe_2$ lattice are varied. For instance, with the defect introduced and the van der Waals gap increased by 6%, we observed a small decrease in the *R*′-factor down to 0.119.

In any event, the simulated diffraction patterns presented in Figs. 6 and 7 for the case of 2*H*/1*T*-$TiSe_2$ do not provide an explanation for the petals observed on the experimental XPD pattern in the polar angle region of 45°–55° (Fig. 3a). A certain advance towards their interpretation occurs, when we take into consideration the small deviation of the real crystal surface from the ideal plane (001) $TiSe_2$. Fig. 8 displays the results of XPD simulation of Se-electrons ($E_{kin} = 1310$ eV) for the surface of 1*T*-$TiSe_2$ with an artificial "bend" of the topmost slab Se–Ti–Se. One can see that as the curvature of the surface increases from 1° to 5° the features in the form of petals in the angle range of 45°–55° are pronounced clearer, although the *R*′-factor of such structures is generally worse than that of an ideal 1*T*-$TiSe_2$ surface. It is evident that the bend of the surface layer should inevitably be associated with its expansion along the basal plane. That, in turn, results in the increase in the lattice parameter a_0 and in the reduction in the ratio c_0/a_0, thus providing the formation of the Se4*p*/Ti3*d*-gap, which is observed by ARPES techniques. Therefore, the surface relaxation model that gives the best agreement between theory and XPD experiment also explains the results of ARPES experiments.

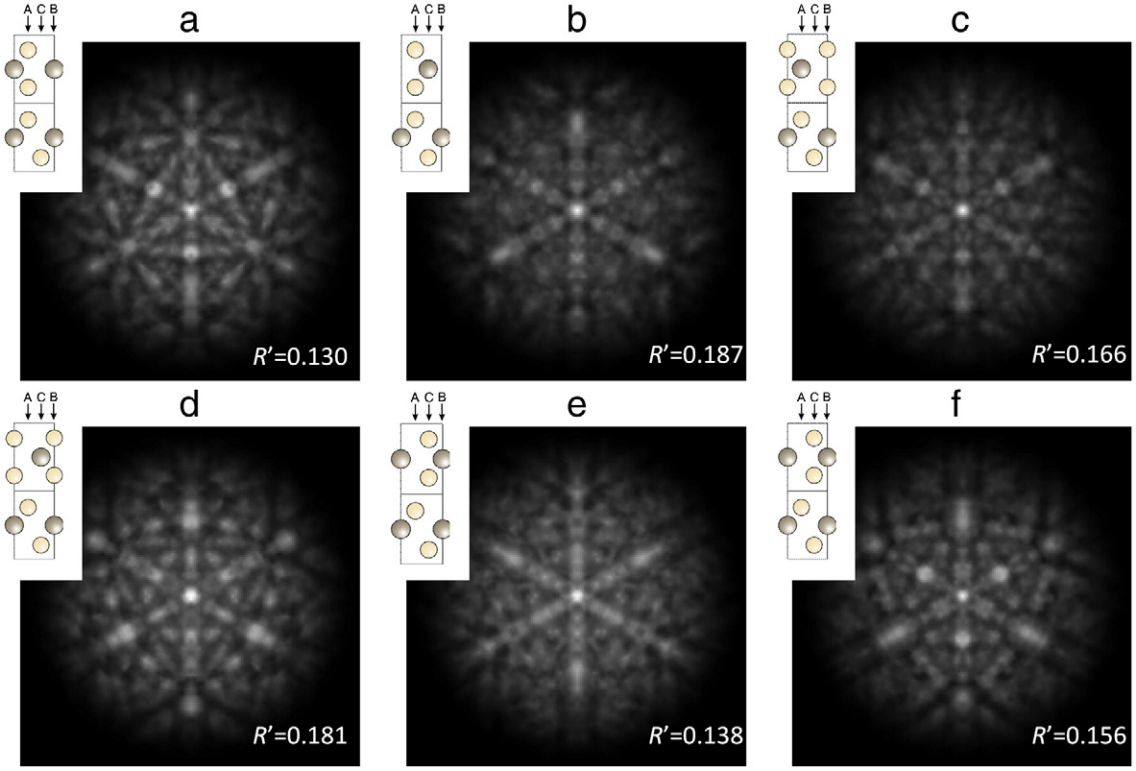

Fig. 6. Theoretical images of photoelectron diffraction patterns of Se-electrons ($E_{kin} = 1310$ eV) simulated for six versions of arrangement of the three-layer slab 2*H*-$TiSe_2$ agreed with the 1*T*-$TiSe_2$ layers below: a — AbA AbC, b — AcA AbC, c — BaB AbC, d — BcB AbC, e — CaC AbC, and f — CbC AbC. Shown on the insets are the sequences in the arrangement of Se and Ti atoms.

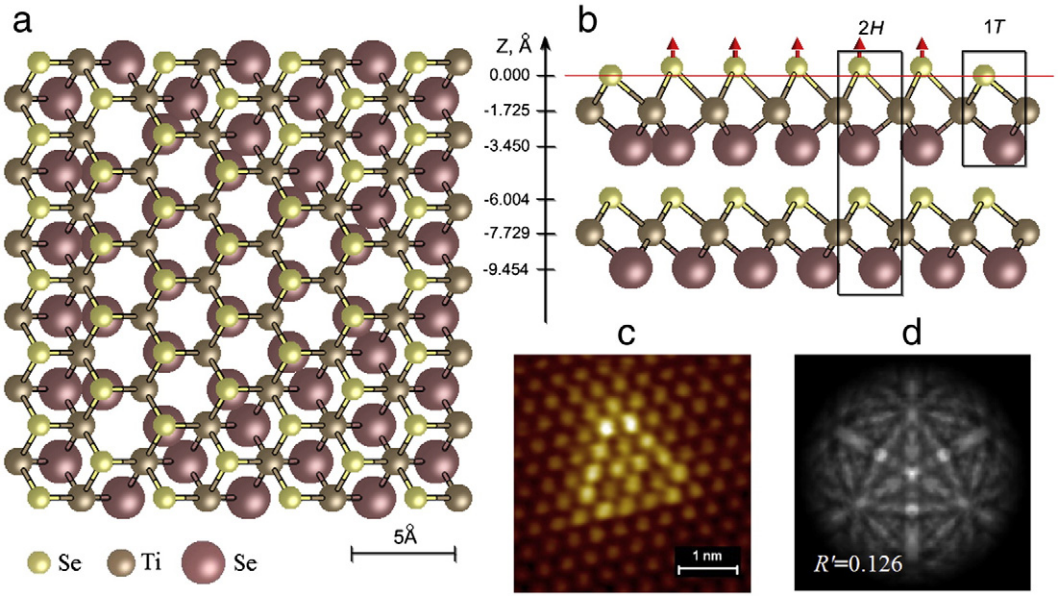

Fig. 7. A model of the 1*T*-$TiSe_2$ surface with a structural defect of 2*H*-$TiSe_2$ type in the first slab at the surface (a, b); a fragment of an *STM* image of the defect on the cleaved surface of 1*T*-$TiSe_2$ crystal (c); a theoretically calculated XPD pattern of Se(*LMM*) emission for a model cluster of 1*T*-$TiSe_2$ with the 2*H*-$TiSe_2$ defect in the first slab at the surface (d).

3.3. Reconstruction of a three-dimensional atomic structure around Se and Ti atoms on the 1T-$TiSe_2$ surface

It is known that the X-ray photoelectron diffraction and Auger diffraction data can be interpreted in terms of holography; and based on the experimental XPD patterns, the surface layer structure can be reconstructed in the real space [34,35]. Traditionally, the methods based on the Fourier transform are applied for this purpose. In the present work we used a SPEA-MEM (Scattering Patterns Extraction Algorithm with Maximum Entropy Method), an alternative approach proposed by T. Matsushita et al. [27,36] for reconstruction of the atomic structure of 1*T*-$TiSe_2$ from the Se(*LMM*) and Ti2*p* diffraction pattern (Fig. 3). For the layered structure of 1*T*-$TiSe_2$, a procedure of translating the atoms in the close-packed layer is realized in the SPEA-MEM algorithm, and interatomic distances are estimated in the surface layer. In order to obtain a more accurate interpretation of experimental holographic images, we carried out reconstruction of model XPD patterns calculated for an ideal structure of 1*T*-$TiSe_2$. Comparative analysis was performed for model and experimental reconstructions to determine the positions of 128 atoms of several surface layers of the $TiSe_2$ cleaved surface. The reconstruction technique is elaborated in [37].

Fig. 9 displays a reconstructed atomic structure of 1*T*-$TiSe_2$ upper layers in the form of an isosurface, which passes through the bulk at 45% of maximum intensity. Because the 1*T*-$TiSe_2$ crystal has a layered structure with the Se–Ti–Se slabs separated by the van der Waals gap, when the (100) surface is formed, one half of the selenium atoms are located in the upper layer, and the other half of selenium atoms are located in the lower layer beneath the layer of titanium atoms. In terms of photoemission, these two positions of selenium atoms are inequivalent and they cannot be distinguished experimentally via adjustments to the corresponding energies of Auger electrons Se(*LMM*).

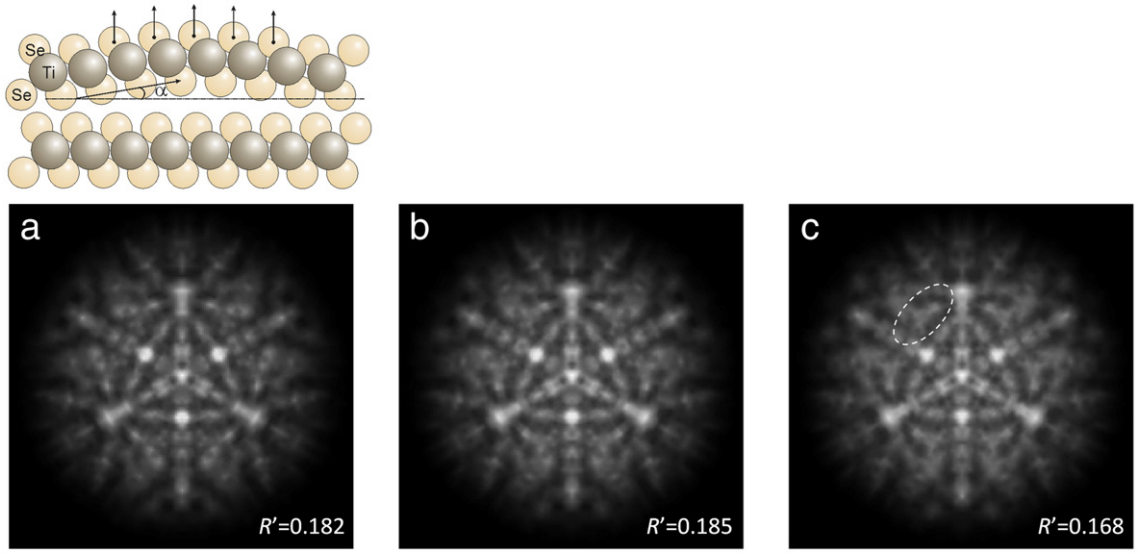

Fig. 8. 1*T*-$TiSe_2$ structure XPD stereographic projections in Se-electrons (E_{kin} = 1310 eV), with the topmost three-layer slab Se–Ti–Se bended outwards from the bulk. The insets display the bended surface layer arrangement; values of the bending angle α: a — 1.72°, b — 3.44°, c — 5.16°.

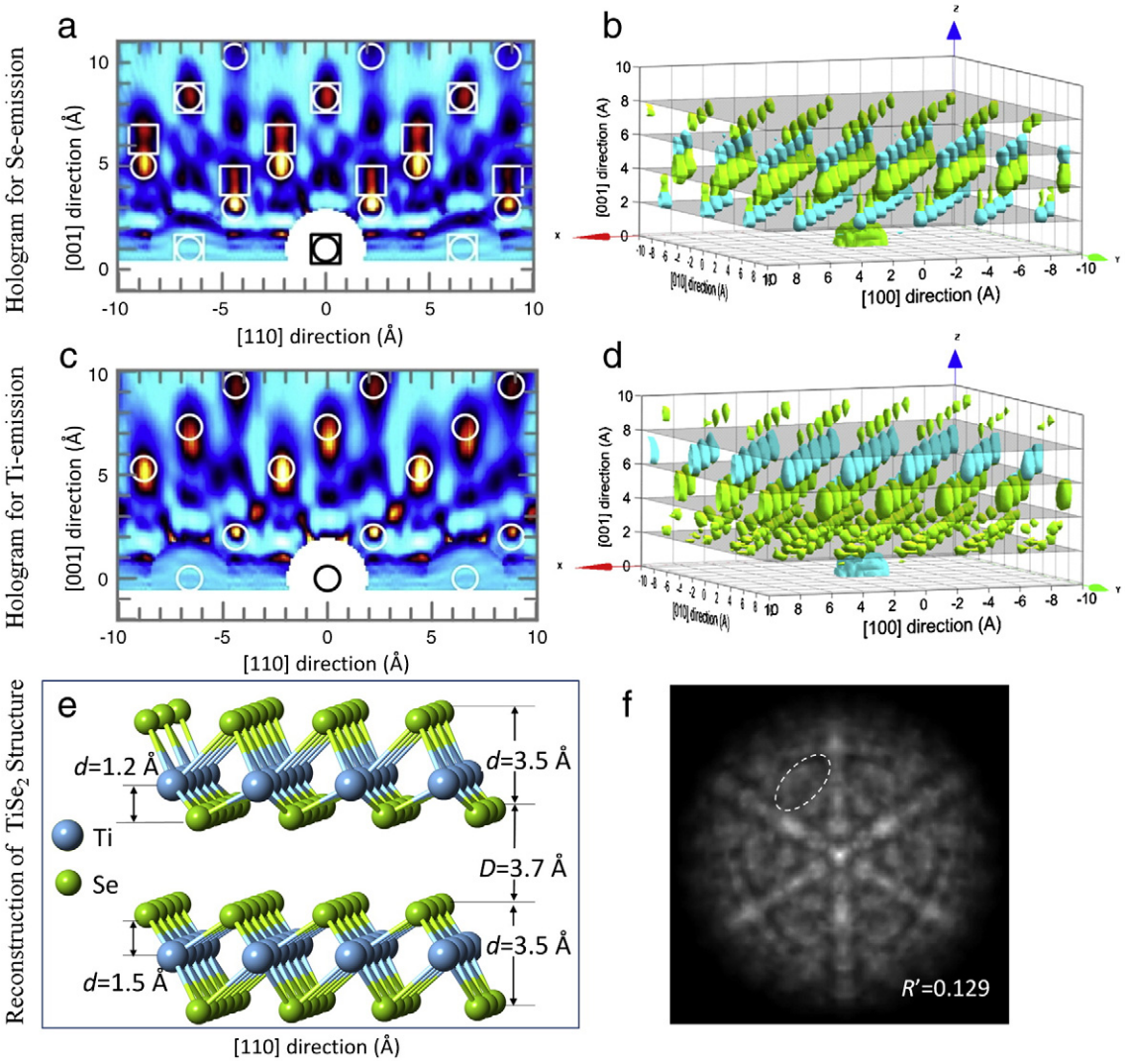

Fig. 9. Reconstructed real space image of the 1*T*-$TiSe_2$ surface layer structure based on the Auger electrons Se(*LMM*) hologram (a, b) and photoelectron hologram Ti2*p* (c, d): a and c represent a section in the *YZ* plane; and *b* and *d* represent a three-dimensional representation. For Se(*LMM*) emission, the reconstructed pattern is a superposition of two images, each of the images corresponds to a fragment of the 1*T*-$TiSe_2$ structure surrounding two inequivalent positions of selenium atoms: (a) denoted with circles are the nearest neighbor atoms around Se^{II}-atom in the lower layer of the Se–Ti–Se^{II} slab; and denoted with squares are the Se nearest neighbor atoms in the upper layer of the Se–Ti–Se^{II} slab. For Ti2*p* emission (c) denoted with circles are the nearest neighbor atoms around Ti-atom. Positions are denoted according to positions in the ideal crystal structure 1*T*-$TiSe_2$. e — a model of 1*T*-$TiSe_2$ surface derived from the two 3*D*-reconstructions of the Auger electrons Se(*LMM*) hologram and photoelectron hologram Ti2*p*; f — a theoretically calculated XPD pattern of Se(*LMM*) emission for this model cluster of 1*T*-$TiSe_2$.

Because the SPEA-MEM algorithm extracts the image of the nearest environment of the emitter atom, the resulted image is obtained in the form of superposition of the two fragments of 1*T*–$TiSe_2$ structure reflecting the nearest environment of selenium atoms in the upper and lower layers. Moreover, the mean free path of Auger electrons Se(*LMM*) (E_{kin} ~ 1200 eV) amounts to $\lambda \approx 21.8$ Å, i.e., there are three slabs at the surface separated with the van der Waals gap that are taken into consideration. For selenium in the upper layer in the second or the third slab, the nearest environment differs from that in the first slab at the surface. In addition, our suggestions regarding the structural distortions in the topmost slab are to be considered. As a result, the total reconstructed pattern for selenium is rather complicated and blurred.

The situation for titanium seems more definite. Firstly, all titanium positions in 1*T*-$TiSe_2$ are equivalent structurally. Secondly, the mean free path of electrons emitted from Ti2*p* levels (E_{kin} ~ 1030 eV) amounts to $\lambda \approx 16.8$ Å, i.e., only two surface slabs of Se–Ti–Se are considered. So, Ti2*p* photoelectron holography allows the structure of surface layer to be reconstructed with a better quality than in the case of XPD pattern of Se(*LMM*) emission. Regardless the fact that in our experiment the XPD pattern of Ti2*p* emission was recorded at a scanning step of 5° over azimuthal and polar angles, the structure of titanium nearest environment reconstructed from the pattern turns out to be more definite and allows interatomic distances to be evaluated for the first two slabs of 1*T*-$TiSe_2$.

According to the holographic reconstruction, the structure of cleaved $TiSe_2$ surface is of 1*T* polytype. Our estimates demonstrate that two topmost slabs of a thickness d ~ 3.5 Å divided by the van der Waals gap D ~ 3.7 Å and the interatomic distance in titanium and selenium layers being a_0 ~ 3.85 Å. In two Se–Ti–Se slabs at the surface, it is revealed that the titanium layers are displaced one towards another along the [001] axis. Relative to the middle of the slab, the titanium layers are displaced in the following manner: in the topmost slab, downward by ~0.55 Å; in the second slab, upward by ~0.25 Å in the normal direction to the surface. It should be taken into consideration that a holographic reconstruction allows visualization of an averaged structure only and is not capable of visualizing point defects or asymmetric features.

Comparing the holographic reconstruction results with the model XPD calculations of $TiSe_2$ surface, the following can be noted. The 3*D*-

reconstructions in the first approximation determine the structural positions of atoms, i.e., set the parameters of the surface structure. Similar parameters are established by means of XPD calculations of model clusters, which are supposed to correspond to the minimum *R*-factor indicating the agreement between theoretical and experimental XPD patterns. In our case, the model calculations provide a number of descriptions of the 1*T*-$TiSe_2$ surface structure. In particular, the model calculations allow a relaxation contraction (expansion) along the *c* axis, alteration of the lattice parameter a_0, structural defects in the form of inclusions of 2*H*-$TiSe_2$ polytype, etc. In the case of a defect-free model, we had to make a choice between two descriptions of the surface structure of 1*T*-$TiSe_2$, which are characterized with differences in the parameters *D* and *d*, and a notably great deference in the parameter a_0. Since the parameter a_0 ~3.83 Å in one of the descriptions is the same as that in the 3*D*-reconstruciton, we accepted the corresponding structural model as most adequate. An additional benefit of this model is the increase of parameter *D* by some 20% relative to the value in the bulk, which is also confirmed by the 3*D*-reconstruction, though on a considerably larger scale (~45%).

There is still an outstanding issue to be solved, which is related to the difference in the estimates of thickness of the topmost slab of Se–Ti–Se in the XPD model pattern and in the 3*D*-reconstruction: in the former case, 14% contraction of the slab is suggested; while in the latter case, thickness of the slab remains essentially constant. This can possibly be associated with the finding that the 3*D*-reconstruction is characterized with an effect of displacement of titanium atoms in the topmost slab from the position in the center to the second layer of selenium. The matter is that selenium atoms of the second layer (Se^{II}), acting as emitters of Auger electrons, provide the greatest contribution into the diffraction pattern of Se(*LMM*) at the expense of the direct scattering on the titanium atoms located above. So, the calculated *R*-factor is especially sensitive to alteration in this very parameter and the effect of contraction of the slab by 14% may reflect the reduction in the Ti–Se^{II} distance inside the slab in the XPD model.

To compare the model built on the basis of 3*D*-reconstructions for Si and Ti with the models considered earlier, an XPD pattern was calculated on Se(*LMM*) (Fig. 9f). It can be seen that the main reflections on the resulted XPD are diffused considerably, which is caused by a number of reasons, in particular, by deviation of titanium positions in the first two slabs off the middle position. Interestingly, expanding of two van der Waals gaps within the model has resulted in the formation of characteristic "petals" (shown as the dash line) similar to those on the XPD pattern (Fig. 3a) and on the pattern calculated for the bended slab model (Fig. 8c). The resulted *R'*-factor of 0.129 is tolerable but far from the minimum value (Fig. 5b), which is caused primarily by impossibility of identifying accurately the positions of atoms judging from the diffuse maxima of holographic patterns in Fig. 9a,c. To optimize the structure within the model built on the basis of the 3*D*-reconstruction, a considerably greater number of parameters is necessary to be varied: apart from *a*, *d* and *D*, due consideration should be given to the thickness of the second slab, the gap between this slab and the third slab, and the position of titanium layers in the two upper slabs.

4. Conclusion

The work presents a study of the 1*T*-$TiSe_2$ surface by scanning tunneling microscopy (STM) and X-ray photo- and Auger electron diffraction (XPD). The atomic structure of 1*T*-$TiSe_2$ surface layers is reconstructed from the XPD pattern of Se(*LMM*) and Ti2*p* emission using the photoelectron holography scattering pattern extraction algorithm with maximum entropy method (SPEA-MEM).

Model calculations of XPD Se(*LMM*) performed for the 1*T*-$TiSe_2$ surface in the multiple scattering approximation have demonstrated a good agreement with the experimental XPD data. The best agreement between theory and experiment was obtained for a model, in which the topmost three-layer slab of Se–Ti–Se structure of titanium diselenide is compressed by ~14%, and, on the contrary, the lattice parameter a_0 is expanded by ~0.3 Å relative to the lattice parameter in the bulk of the crystal, and the van der Waals gap between the structural slabs increased by ~19%. As an alternative, a possibility has been considered that defects in the form of 2*H*-$TiSe_2$ are present in the structure of 1*T*-$TiSe_2$. The presence of such defects on the surface of titanium dichalcogenide is supported by the STM data available and by quantum-chemical calculations [29]. It has been established that when a structural defect in the form of 2*H* polytype is introduced into a model cluster of 1*T*-$TiSe_2$ the theoretically calculated XPD pattern of Se(*LMM*) emission also shows a good agreement with the experiment. Additionally, a version has been considered of bending the topmost three-layer slab away from the bulk. In this case, we failed to considerably improve the *R*-factor indicating the agreement of model XPD calculations with experiment, yet the XPD pattern demonstrate more clearly the features in the form of petals in the angle range of 45°–55°.

The holographic 3*D*-reconstructions of the cleaved surface of $TiSe_2$ determine the 1*T* polytype of the surface. The diffuse character of the 3*D*-reconstruction does not allow the diselenide lattice parameters to be established accurately, and the presence of two components (Ti and Se) and the layered structure complicate general interpretation of the pattern. Our evaluations demonstrate that two surface slabs Se–Ti–Se have a thickness *d* ~3.5 Å (~1%) and are divided by the van der Waals gap *D* ~3.7 Å (+45%); the interatomic distance in the titanium and selenium layer inside the topmost slab is a_0 ~3.85 Å (+0.3 Å). It has been established that the titanium layers are displaced relative to the middle of the slab in the following manner: in the upper slab, downward by 0.55 Å; in the second slab, upward by 0.25 Å in the normal direction to the surface. In general, the results of the 3*D* reconstruction agree with the data obtained in XPD pattern simulation. In both cases, on the surface of 1*T*-$TiSe_2$ an increase is observed in the lattice parameter a_0 and in the van der Waals gap between two surface slabs. The difference in the thickness estimates for the topmost slab Se–Ti–Se is attributed to the effect of Ti layer approaching the lower selenium layer Se^{II}. Since it is these two layers that give the greatest contribution into the diffraction pattern of Se(*LMM*), the simulated XPD calculations with the *R*-factor analysis may mimic contraction of the whole slab.

Therefore, the experimental investigations provide evidence in favor of deformation of the upper layers of the fresh cleaved surface of 1*T*-$TiSe_2$ single crystal. Such deformation of the surface layer structure can be explained by relaxation effects on the surface of the 1*T*-$TiSe_2$ crystal, by the defects present on the surface and under the surface, and by deviation of the real surface geometry from the (001) plane of the crystal, for instance, at the expense of spalling of the topmost Se–Ti–Se slab off the crystal matrix or due to growth defects deeper in the crystal. Distortion of the crystal lattice in the topmost layer of 1*T*-TiX_2 (X:S,Se) dichalcogenides in the form of expansion along the basal plane or contraction along the normal to that plane can result in a decrease in the c_0/a_0 ratio thus providing an ARPES-observable energy gap between the Se(S)*p*- and Ti3*d*-bands.

Acknowledgments

The work was supported by the Russian Foundation for Basic Research (grants nos. 10-03-96047, 11-03-00063) and Presidium of the Ural Branch of Russian Academy of Sciences (grants nos. 12-M-23-2010, 12-P-3-1015, 12-U-3-1006).

References

[1] In: D. Baeriswyl, L. Degiorgi (Eds.), Strong Interactions in Low Dimensions, Physics and Chemistry of materials with low-dimensional structures, Springer-Verlag, 2010, p. 447.

[2] In: H.P. Hughes, H.I. Starnberg (Eds.), Electron Spectroscopies Applied to Low-Dimensional Structures, Physics and Chemistry of Materials with Low-Dimensional Structures, Kluwer Academic Pub., 2000, p. 504.
[3] J. Rouxel, In: in: F.A. Levy (Ed.), Intercalated Layered Materials, Reidel, Dordrecht, 1979, p. 201.
[4] E. Amzallag, I. Baraille, H. Martinez, M. Rérat, D. Gonbeau, J. Chem. Phys. 128 (2008) 014708.
[5] E. Amzallag, H. Martinez, I. Baraille, M. Rerat, M. Loudet, D. Gonbeau, Solid State Sci. 9 (2007) 594.
[6] H. Wang, J. Lee, M. Dreyer, B.I. Barker, J. Phys. Condens. Matter 21 (2009) 265005.
[7] H. Katzke, P. Toledano, W. Depmeier, Phys. Rev. B 69 (2004) 134111.
[8] Y. Tison, H. Martinez, I. Baraille, M. Loudet, D. Gonbeau, Chem. Phys. 290 (2–3) (2003) 267.
[9] G.P.E.M. van Bakel, J.Th.M. De Hosson, Phys. Rev. B 46 (4) (1991) 2001.
[10] H. Murata, K. Kataoka, A. Koma, Surf. Sci. 478 (3) (2001) 131.
[11] R.V. Coleman, Zhenxi Dai, W.W. McNairy, C.G. Slough, Chen Wang, In: in: G. Benedek (Ed.), Physics and Chemistry of Materials with Low-Dimensional Structures, vol. 16, Springer, Netherlands, 1992, p. 27.
[12] C.G. Slough, B. Giambattista, A. Johnson, W.W. McNairy, C. Wang, R.V. Coleman, Phys. Rev. B 37 (1988) 6571.
[13] H. Cercellier, C. Monney, F. Clerc, C. Battaglia, et al., Phys. Rev. Lett. 99 (2007) 146403.
[14] T. Rohwer, S. Hellmann, M. Wiesenmayer, et al., Nature 471 (2011) 490.
[15] K. Rossnagel, J. Phys. Condens. Matter 23 (2011) 213001.
[16] A. Zunger, A.J. Freeman, Phys. Rev. B 16 (2) (1979) 906.
[17] J.J. Barry, H.P. Hughes, P.C. Klipstein, R.H. Friend, J. Phys. C: Solid State Phys. 16 (1983) 393.
[18] C. Monney, E.F. Schwier, M.G. Garnier, N. Mariotti, C. Didiot, H. Cercellier, J. Marcus, H. Berger, A.N. Titov, H. Beck, P. Aebi, New J. Phys. 12 (2010) 125019.
[19] R.H. Friend, D. Jerome, W.Y. Liang, J.C. Mikkelsen, A.D. Yoffe, J. Phys. C 10 (1977) L705.
[20] C.M. Fang, R.A. de Groot, C. Haas, Phys. Rev. B 56 (8) (1997) 4455.
[21] R.H. Friend, A.D. Yoffe, Adv. Phys. 36 (1) (1987) 1.
[22] A.H. Reshak, S. Auluck, Phys. Rev. B 68 (2003) 245113.
[23] C.S. Fadley, In: in: R.Z. Bachrach (Ed.), Synchrotron Radiation Research: Advances in Surface and Interface Science, vol. 1, Plenum Press, New York, 1992, p. 421.
[24] C. Westphal, Surf. Sci. Rep. 50 (2003) 1.
[25] E.V. Shalaeva, M.V. Kuznetsov, J. Struct. Chem. 44 (3) (2003) 465.
[26] F.J. Garcia de Abajo, M.A. Van Hove, C.S. Fadley, Phys. Rev. B 63 (7) (2001) 075404.
[27] A. Uesaka, K. Hayashi, T. Matsushita, S. Arai, Phys. Rev. Lett. 107 (4) (2011) 045502.
[28] T. Matsushita, F.Z. Guo, F. Matsui, Y. Kato, H. Daimon, Phys. Rev. B 75 (2007) 085419.
[29] A.S. Razinkin, A.N. Enyashin, T.V. Kuznetsova, A.N. Titov, M.V. Kuznetsov, A.L. Ivanovskii, J. Struct. Chem. 51 (4) (2010) 737.
[30] D. Stoltz, S.E. Stoltz, Physica B 398 (2007) 172.
[31] R.S. Saiki, A.P. Kaduwela, M. Sagurton, et al., Surf. Sci. 282 (1993) 33.
[32] M.A. Van Hove, S.Y. Tong, M.H. Elconin, Surf. Sci. 64 (1977) 85.
[33] L. Despont, F. Clerc, M.G. Garnier, H. Berger, L. Forro, P. Aebi, Eur. Phys. J. B 52 (3) (2006) 421.
[34] J.J. Barton, Phys. Rev. Lett. 67 (1991) 3106.
[35] S. Omori, Y. Nihei, E. Rotenberg, J.D. Denlinger, S. Marchesini, S.D. Kevan, B.P. Tonner, M.A. Van Hove, C.S. Fadley, Phys. Rev. Lett. 88 (2002) 055504.
[36] T. Matsushita, F. Matsui, H. Daimon, K. Hayashi, J. Electron Spectrosc. Relat. Phenom. 178–179 (2010) 195.
[37] I.I. Ogorodnikov, A.S. Vorokh, A.N. Titov, M.V. Kuznetsov, JETP Lett. 95 (7) (2012) 372.